On the use of pixelated plastic scintillator and silicon photomultipliers array for coded aperture gamma-neutron imaging

Clement Lynde, Camille Frangville, Romuald Woo, Vincent Schoepff, Guillaume H. V. Bertrand, Jean-Michel Bourbotte, Matthieu Hamel, Jonathan Dumazert, Frédérick Carrel

On the use of pixelated plastic scintillator and silicon photomultipliers array for coded aperture gamma-neutron imaging

C. Lynde, C. Frangville, R. Woo, V. Schoepff, G. H. V. Bertrand, J.-M. Bourbotte, M. Hamel, J. Dumazert, F. Carrel

Abstract— **We report the investigations made on the use of pixelated plastic scintillator (PS) and silicon photomultipliers (SiPM) array applied to coded aperture gamma-neutron imaging. Specifically, verification of the ability of a multiplexing readout to discriminate and localize neutron interactions was studied.**

In its intended configuration, the gamma-neutron imager design consists of a coded aperture aligned with a matrix of 12×12 PS each coupled to a SiPM. The coded aperture is a rank 7 modified uniformly redundant array (MURA), composed of 1.2 cm of tungsten, with a surface area of 100.4 mm×100.4 mm and placed at 5 cm from the detector. The pixelated PS is composed of polystyrene and standard fluorophores (20 wt% PPO, 0.03 wt% POPOP) loaded with a lithium carboxylate (Li α-valerate) [1], which allows the triple discrimination between thermal neutrons, fast neutrons and photons. Each pixel of PS has a dimension of 3.6 mm×3.6 mm×3.6 mm and they are separated from each other by 0.6 mm of polytetrafluoroethylene (PTFE). The photonic and electronic readout consists of the ArrayC-30035-144P SiPM from SensL connected to the diode coupled charge division readout from AiT.

First, this neutron imager design was modeled and simulated using the MCNP6 Monte Carlo code. The encoding capability, field of view, and spatial resolution of the neutron imager were therefore evaluated by simulation. Then, we detailed the experimental setups implemented to demonstrate the feasibility of coupling pixelated plastic scintillator to SiPM to localize radioactive sources and showed the results obtained. Finally, based on this position-sensitive gamma-neutron detector, a gamma-neutron imager was prototyped and tested.

Index Terms— **Neutron imaging, Fast and thermal neutrons and gamma-rays discrimination, Pixelated plastic scintillator, SiPM array**

I. Introduction

In the nuclear field, the development of instruments for measuring radioactivity and more particularly imaging systems for locating radioactive materials is an important issue. This need for localization can be found in many areas of the nuclear industry (decommissioning, waste management and radiation protection) as well as for Homeland Security applications (nonproliferation of nuclear material), for the management of nuclear accidents or for nuclear research (Generation IV and fusion reactors). Gamma imaging is currently the most mature technique and several systems such as iPIX [2], Polaris-H [3], ASTROCAM 7000HS [4], RadCam [5], NuVision [6] are commercially available, meanwhile for neutrons, there are to date no equivalent industrialized systems. Several prototypes [7]–[16] were investigated and developed over the last forty years and have demonstrated the feasibility of implementing localization methods for neutron imaging. Nevertheless, significant improvements in either sensitivity or portability still need to be performed to achieve performances that meet the needs of the nuclear industry. This work presents research on the use of plastic scintillators (PSs) coupled with silicon photomultipliers (SiPMs) to achieve good neutron sensitivity while keeping a small footprint. In particular, our work focused on the implementation of a readout system based on low-cost and off-the-shelf components.

II. Coded Aperture Imaging Design

A. Monte Carlo model

The neutron imager design, as shown in Fig. 1 consists of a coded aperture aligned with a matrix of 12×12 plastic scintillators each (as described below) coupled to a silicon photomultiplier. The coded aperture is a rank 7 modified uniformly redundant array (MURA) [17], composed of 10 mm of natural tungsten and 2 mm of natural cadmium for a surface area of 100.4 mm×100.4 mm. The mask was placed 5 cm from the detector so that the fully coded field-of-view (FoV) is a square with a diagonal of 68°. The rank 7 MURA was chosen because, according to our gamma-imaging experience [18], it offers the best compromise between a satisfactory spatial resolution, a relatively short measurement time with little reconstruction noise. The pixelated PS is a 12×12 matrix composed of polystyrene and standard fluorophores loaded with a ^{6}Li carboxylate (typically 72.8%$_{wt}$ styrene, 8.09%$_{wt}$ methacrylic acid, 2.43%$_{wt}$ ^{enriched}Li α-valerate, 16.66%$_{wt}$ 2,5-diphenyloxazole (PPO), 0.02%$_{wt}$ 1,4-bis(5-phenyl-2-oxazolyl)benzene (POPOP)) as recently reported [1]. This composition allows the triple discrimination of thermal neutrons, fast neutrons and photons. Each pixel of PS has

"This work was supported in part by the ANR under Project N° ANR-20-C839-0015-01."

C. Lynde, C. Frangville, R. Woo, V. Schoepff, G. H. V. Bertrand, J.-M. Bourbotte, M. Hamel, F. Carrel is with with the Université Paris-Saclay, CEA, List, F-91120 Palaiseau, France (corresponding author: clement.lynde@cea.fr).

J. Dumazert, was with the Université Paris-Saclay, CEA, List, F-91120 Palaiseau, France. He is now with the CEA-DAM DIF, Arpajon, France.

Orcid number: 0000-0003-0081-2757 (CL), 0000-0003-2527-2371 (CF), 0000-0001-9910-6128 (VS), 0000-0002-3499-3966 (MH), 0000-0003-2444-3263 (JD), 0000-0001-5927-9884 (FC)

dimensions of 3.6×3.6×3.6 mm^3, and the different pixels are separated from each other by 0.6 mm of PTFE. The dimensions were chosen to match those of the ArrayC-30035-144P SiPM from SensL [19].

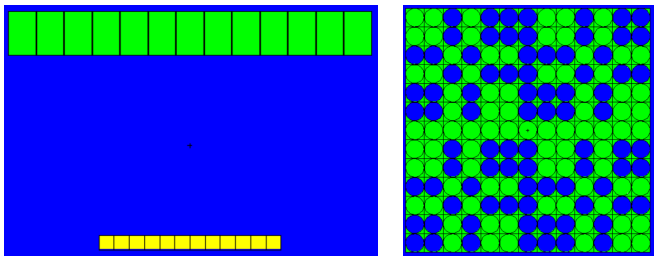

Fig. 1. Illustrations of the MCNP6 model. (a) Sagittal section of the coded aperture imager. (b) Frontal section of the coded mask.

B. Simulation results

The simulated source corresponds to an isotropic ^{252}Cf neutron source [20]. The distance between the centered source and the surface of the coded aperture was set to 50 cm. Fig. 2a shows the projection of the neutron flux through the coded mask on the pixelated scintillator with a simulated particle number (NPS) of 10^8 and Fig. 2b with 10^{10}.

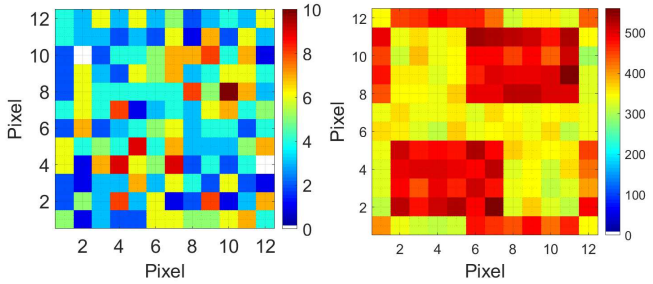

Fig. 2. Raw images of the neutron flux emitted by a ^{252}Cf neutron source through a rank 7 MURA mask on a 12×12 pixelated PS (a) with NPS = 10^8 and (b) with NPS = 10^{10}. Colorbars unit: events.

The mask/anti-mask (90° rotation) method was applied [21]. The decoding process used in this work is the correlation of the raw image with the decoding array, proposed by Gottesman and Fenimore [17]. Fig. 3a shows the decoded image, in the fully coded FoV, with a total number of simulated particle of $2×10^8$ and Fig. 3b with $2×10^{10}$. The spatial resolution (full width half maximum of the hot spot) was evaluated at 7°.

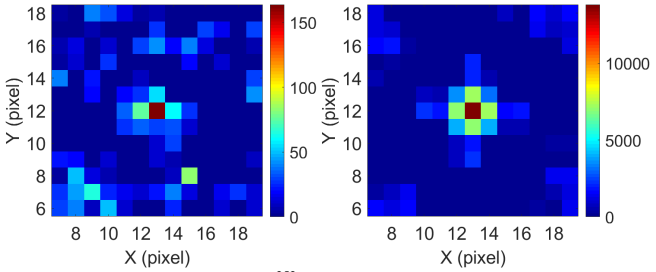

Fig. 3. 2D decoded images of a ^{252}Cf neutron source placed at 50 cm (a) with NPS=$2×10^8$ and (b) with NPS=$2×10^{10}$. Colorbars unit: reconstructed events.

As expected, the noise decreases as the number of detected particles increases but about 1200 neutrons (NPS=$2×10^8$) were sufficient for a good quality image (more visible on Fig. 4). In Fig. 4b, the highest noise value is only half the hot spot of the source.

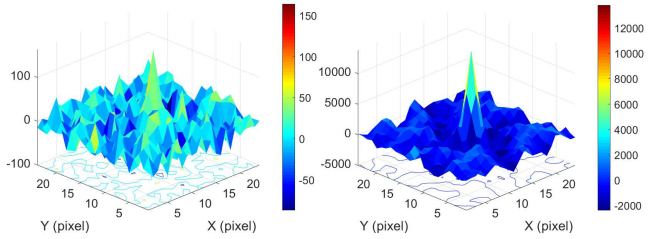

Fig. 4. 3D decoded images of a ^{252}Cf neutron source placed at 50 cm (a) with NPS=$2×10^8$ and (b) with NPS=$2×10^{10}$. Colorbars unit: reconstructed events.

III. Position Sensitive Neutron Detector

A. Materials and Methods

1) SiPM array and plastic scintillators

The dimensions of manufactured plastic scintillators were chosen to match either the ArrayC-30035-16P SiPM or the ArrayC-30035-144P from SensL [19]. Those SiPM arrays were selected because they have gaps between the pixels that allow reflective materials between the scintillators. Optical grease was used to connect the PSs and the SiPM arrays. The PSs #1.1 and #1.2 presented in Fig. 5 were monolithic and composed of chemicals allowing the discrimination of fast neutrons from gamma rays [22]. PS #1.1 (Fig. 5a) was 12 mm×12 mm×10 mm and covered by PTFE for the measurement (Fig. 5b). PS #1.2 (Fig. 5c) was a resized version of PS #1.1 where the thickness was reduced to 3 mm.

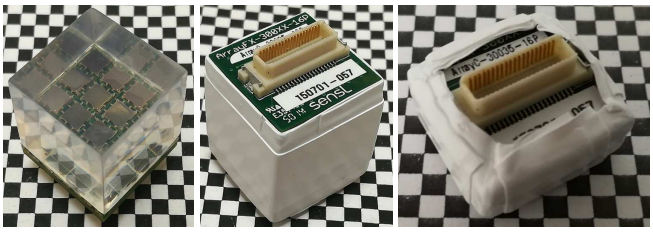

Fig. 5. Monolithic PS. (a) uncovered PS #1.1. (b) PTFE covered PS #1.1. (c) PTFE covered PS #1.2.

Two approaches were attempted to manufacture pixelated PS. The chemical composition used for those PSs was a previously reported ^6Li-doped PS with fast/thermal neutron and gamma ray discrimination capabilities [1]. The first approach was based on a mechanical fabrication of small distinct pixels obtained from a monolithic PS. Each pixel was cut, polished and assembled to form the desired matrices, PS #2.1 and #2.2 and #2.3 as showed in Fig. 6.

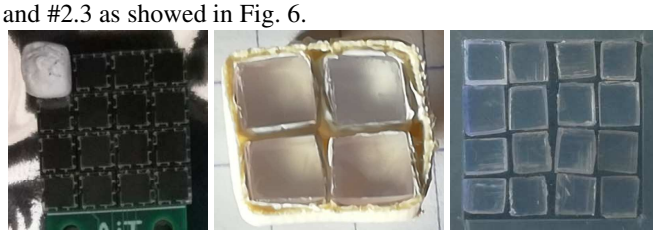

Fig. 6. Pixelated PS. (a) 1×1 PS #2.1. (b) 2×2 PS #2.2. (c) 4×4 PS #2.3.

The second approach involved a direct polymerization of the PS inside an *ad hoc* PTFE mold. Therefore the mold was designed in order to precisely fit the ArrayC-30035-16P SIPM detection cells, such as each pixelated PS has dimensions of 3 mm×3 mm×3 mm. 1 mm of PTFE was used to separate the light response of each pixel. A digital model of the mold was

made on SolidWorks® (Fig. 7a) and several mold batches were machined (Fig. 7b). Finally, the mold was added at the bottom of a glass vial filled with a previously degassed solution of monomers and fluorophores (typically 72.8%$_{wt}$ styrene, 8.09%$_{wt}$ methacrylic acid, 2.43%$_{wt}$ ^{enriched}Li α-valerate, 16.66%$_{wt}$ PPO, 0.02%$_{wt}$ POPOP). The bottle was then sealed under an argon atmosphere before a thermally initiated polymerization took place for curing temperatures between 60–110 °C. PS #3 (Fig. 7c) was then obtained by cutting the excess of scintillating plastic and polished.

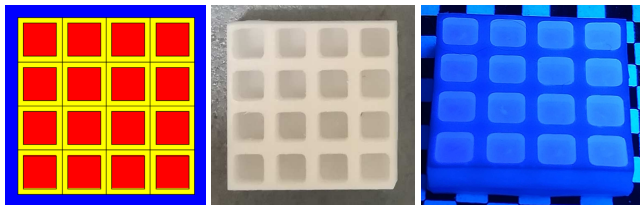

Fig. 7. 4×4 pixelated PS. (a) digital model. (b) final mold. (c) manufactured PS #3 exposed to UV light.

This second approach was used for a large 12×12 PS matrix (Fig. 8). For this PS #4, each pixelated PS has dimensions of 3.6 mm×3.6 mm×3.6 mm and 0.6 mm of PTFE was used to separate the light response of each pixel. The chemical composition is identical to that of PS #3, but without the ^{enriched}Li α-valerate.

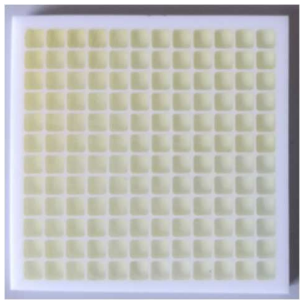

Fig. 8. 12×12 pixelated PS #4.

2) Electronic readouts

In order to minimize the number of channels to be digitized, we used a multiplexing readout from AiT [22],[23], which reduced the 16-channels or 144-channels input to four "position" signals and one "sum" signal. This readout implements a diode-coupled symmetric charge division (DCSCD) circuit dedicated to SiPM. It was originally developed for nuclear medicine imagers, where SiPM replace PMT and the scintillators are inorganic crystals. To the best of our knowledge, it has never been tested on organic scintillators for parallel gamma-neutron localization and discrimination. With a modular approach, AiT has decomposed the overall acquisition chain into three boards (Fig. 9). The "amplifier board power supply" (ABPS) provides the bias voltage for the SiPM and the +5V and -5V voltages for the amplifiers. The "4-channel active base" (AB4) encodes the SiPM signals into four encoded position signals. The "4-channel active base receiver" (ABR4) interconnects the ABPS and the AB4 and sums the four encoded signals. The measurements of the four "position" signals and the "sum" signal were performed with a CAEN "DT5743" digitizer operating at 400 mega-samples/s. The trigger was applied to the sum signal.

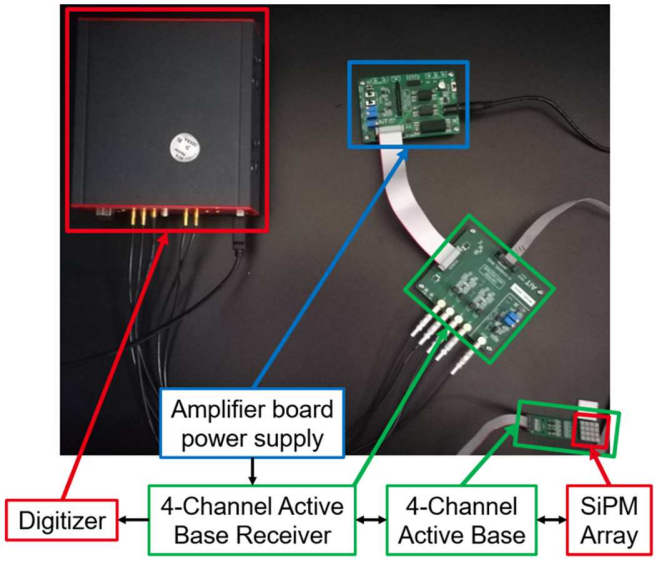

Fig. 9. Acquisition chain with the multiplexing readouts from AiT and digitizer from CAEN.

3) Signal processing

The DCSCD circuit is based on the row/column readout of the Symmetric Charge Division (SCD) [25] circuit. The incoming signal of each SiPM is split through a two diodes chain into one row and one column and each row and column has a separate fast amplifier. Therefore, the original SiPM signal is divided into two X (X^+ and X^-) and two Y (Y^+ and Y^-) signals by a specific combination of values according to its position. To decode the position of the original signal, an algorithm similar to Anger logic [26] was used by combining the four signals values using (1).

$$X = \frac{X^+ - X^-}{X^+ + X^-} \qquad Y = \frac{Y^+ - Y^-}{Y^+ + Y^-}, \tag{1}$$

The pulse shape discrimination (PSD) principle used in this work is the charge comparison method (CCM) [27]. This method is based on ratios of pulse integrals over two different time periods and was applied to the "sum" signal. Those integral durations were optimized according to the procedure proposed in [28].

4) Radioactive sources

We used four radioactive sources sealed in metal or plastic capsules to test the system and its components: ^{133}Ba, ^{22}Na, ^{137}Cs, ^{241}Am and ^{252}Cf.

TABLE I
RADIOACTIVE SOURCES.

Radionuclide	Emission of interest	Activity
^{133}Ba	γ: 81 keV and 356 keV	19.5 MBq
^{22}Na	γ: 511 keV and 1.27 MeV	742 kBq
^{137}Cs	γ: 662 keV	468 kBq
^{241}Am	γ: 59.5 keV and 5.49 MeV	37 MBq
^{252}Cf	Neutron: average energy of 2.1 MeV [20]	6.5×10^4 n.s^{-1}

B. Experimental results

1) Spatial response

The ^{133}Ba source was used for the spatial response tests. The source was aligned with the center of the SiPM matrix and

placed at 50 cm from the surface of the PS. The first tests were performed with the monolithic PS #1.1 (Fig. 10a). We found the results to be inconclusive because the light was homogeneously distributed over the SiPM matrix, either due to the scintillator thickness or due to its non-pixelated state. The results with the PS #1.2 (Fig. 10b) showed that the reduction in thickness was not sufficient.

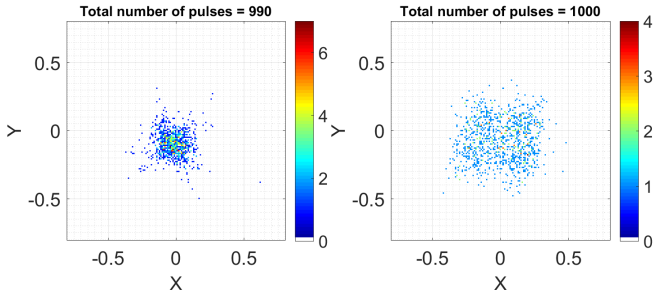

Fig. 10. 2-D position map of pulses induced by a ^{133}Ba photon source (a) within the PS #1.1, (b) within the PS #1.2. Colorbars unit: events.

On the other hand, tests carried out with pixelated PS were significantly more conclusive. In Fig. 11, the 2-D maps of the positions calculated from the signals is representative of the number and positioning of the scintillators on the SiPM matrix. One can clearly distinguish the pixelization of the detection. In contrast, it can be observed on Fig. 11c that the counting is not evenly distributed in the image for the assembled PS #2.3, whereas it is definitely more consistent with the molded PS #3 (Fig. 12). We explain this inhomogeneity mainly due to the non-uniformity of the SiPM gain factor within the array, and to a lesser extent of the PS pixel light yield. These results remained extremely promising and were adjusted by using an equalization matrix. Fig. 13 shows that all 144 pixels of the PS #4 can be identified when exposed to the ^{133}Ba source positioned 50 cm from the surface of the PS.

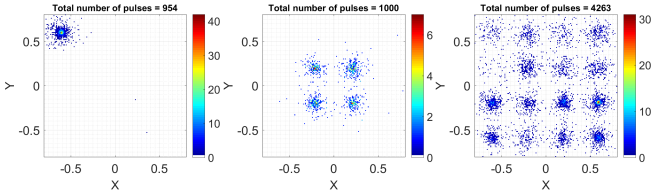

Fig. 11. 2-D position map of pulses induced by a ^{133}Ba source. (a) within the PS #2.1. (b) within the PS #P2.2. (c) within the PS #2.3. Colorbars unit: events.

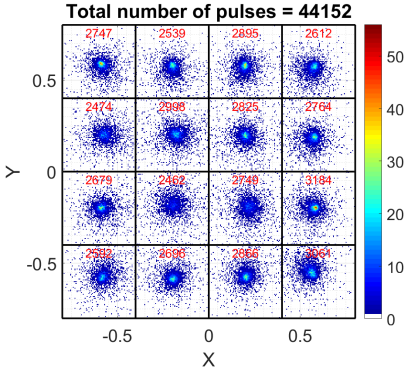

Fig. 12. 2-D position map of pulses induced by a ^{133}Ba source within the PS #3. Colorbars unit: events.

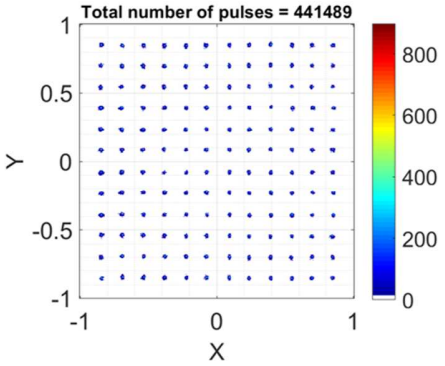

Fig. 13. 2-D position map of pulses induced by a ^{133}Ba source within the PS #4. Colorbars unit: events.

2) *Energy response*

Spectral measurements were performed with ^{22}Na and ^{137}Cs sources, and are presented in Fig. 9. The Compton edges of ^{22}Na at 341 keV and 1062 keV, and of ^{137}Cs at 477 keV, were not assessable when the whole matrix ("_Full" solid lines in Fig. 14) was measured. However, they started to become visible when only one pixel ("_Mono" dotted lines in Fig. 14) was measured. These results confirmed that the non-uniformity of the SiPM gain factor is of great importance. A first approximate calibration was nevertheless carried out based on these spectra.

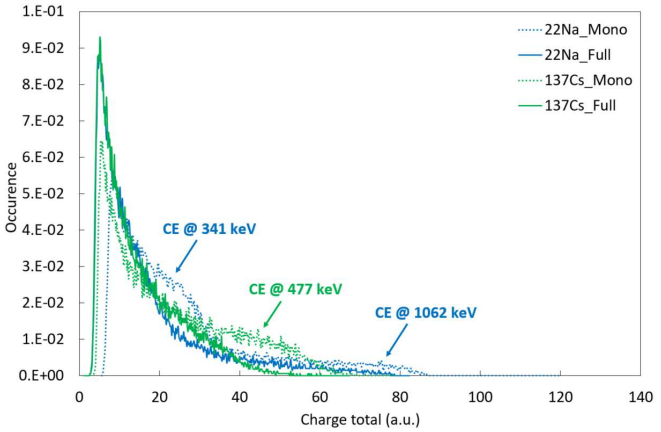

Fig. 14. Energy spectra of PS #3 with ^{22}Na and ^{137}Cs sources. "Mono" corresponds to one pixel of the PS and "Full" to the full matrix.

3) *Triple fast/thermal neutron and gamma discrimination*

To illustrate the possibility to assess the triple discrimination with the pixelated PS #3, the classical biparametric histogram was obtained with a non-thermalized (Fig. 15a) and thermalized by 5 cm of polyethylene (Fig. 15b) ^{252}Cf source. The results showed the appearance of an ovoid area caused by the ions generated after the capture of a thermal neutron by a ^{6}Li nucleus. These results thereby exhibit a triple discrimination of n_{th}/n_{fast}/gamma reached with the PS #3. For an energy range above around 250 keVee, a n_{fast}/gamma Figure of Merit of 0.90 was measured with PS #3 and of 0.71 with PS #4 (Fig. 16).

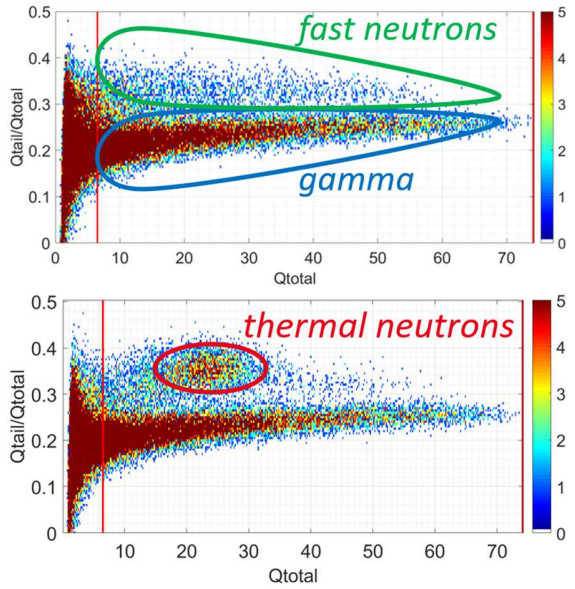

Fig. 15. Biparametric histogram of tail-to-total integral as a function of the total integral obtained with a ^{252}Cf source and the PS #3. (a) non-thermalized. (b) thermalized. Colorbars unit: events.

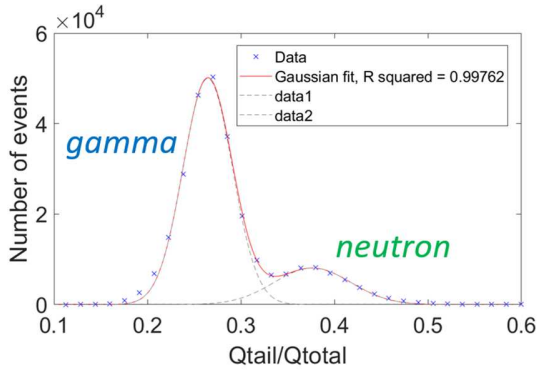

Fig. 16. Histogram of the tail-to-total integrals obtained with a ^{252}Cf source and the PS #4.

4) Neutron detection efficiency

Two geometries, the 4×4 PS #3 and the 12×12 PS #4, were simulated and compared to our previous pixelated neutron detector based on Timepix [29]. The simulated and experimental source was a ^{252}Cf isotropic source placed at 15 cm from the surface of the detector.

The gain evaluated in Table II is the ratio between the count rate obtained with the new configurations and the one obtained with the neutron-enhanced Timepix. For the 4×4 pixelated PS geometry, the results showed a gain of neutron sensitivity of 28 compared to Timepix detector, which is confirmed with a slight decrease by the measurements. The experimental results indicated a gain of about 100 with the 12×12 configuration while the simulation gave an expected gain of 370. We explain this difference by the potential difference in energy threshold and the non-perfect discrimination performance.

TABLE II
COMPARISON OF NEUTRON SENSITIVITY PERFORMANCE BETWEEN NEW CONFIGURATIONS WITH PLASTIC SCINTILLATOR AND THE NEUTRON-ENHANCED TIMEPIX DETECTOR.

Setup	Gain on neutron detection total efficiency	
	Simulation	Experiment
PS #3	28×	25×
PS #4	370×	100×

5) Source localization tests

To further verify the possibility of locating source with this acquisition chain, two experiences have been set up. The first one consisted of the ^{252}Cf source placed 3 mm away from a corner of the detector surface. Fig. 17 represents the spatial distribution of 9100 pulses detected in 5 min, in this configuration. We can clearly see a higher counting rate evidencing the location of the source at the top left of the pixelated detector which is in well agreement with the position of the source.

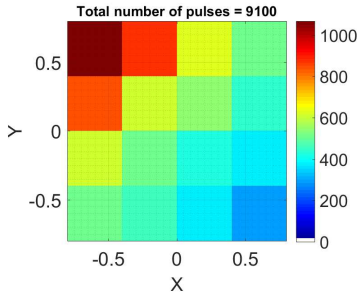

Fig. 17. Spatial distribution of events induced by a ^{252}Cf source placed at the top left corner of PS #3. Colorbars unit: events.

The second configuration associated a tungsten pinhole with PS #3, as shown in Fig. 18. A ^{241}Am source and a ^{252}Cf source were placed at different positions in the FoV of the pinhole. Fig. 19 shows the spatial distribution of pulses classified in three categories according to their energy and their origin. Fig. 19a corresponds to low-energy photons (<100 keV) and the ^{241}Am source is mainly visible there. Fig. 19b consists of high-energy photons (>250 keV) and only the ^{252}Cf source is visible. Fig. 19c, the particles discriminated to acquire this image were fast neutrons and as expected the ^{252}Cf source is the exclusive result.

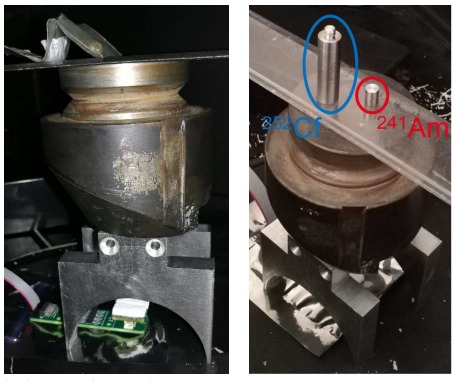

Fig. 18. Pinhole experimental setup.

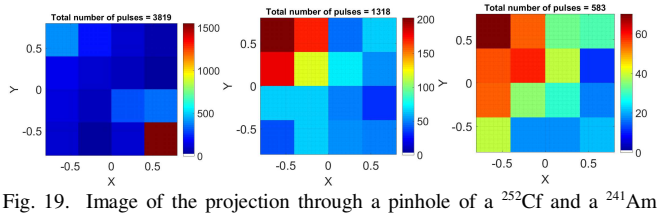

Fig. 19. Image of the projection through a pinhole of a ^{252}Cf and a ^{241}Am sources. (a) Low-energy photons. (b) High-energy photons. (c) Fast neutrons. Colorbars unit: events.

IV. Gamma-Neutron Imager

A. Prototype setup

The imager (Fig. 20) part of our prototype consists of the association of:

1) Rank 7 MURA coded aperture made of 1.5 cm of polyethylene,
2) PS #4,
3) ArrayC-30035-144P,
4) AB4 electronic readout.

For reasons of cost and ease of manufacture, the first mask of the prototype was made of polyethylene instead of tungsten and cadmium. Those four components were assembled in a polyethylene camera body with an external dimension of 17 cm×14 cm×9 cm (height × width × depth) and a mass of 800 grams. An optical camera was placed on top of the imager but was not used for the experiments.

Fig. 20. Prototype of the gamma-neutron imager based on pixelated plastic scintillator and coded aperture.

B. Neutron source response

Fig. 21 shows the result obtained with the ^{252}Cf neutron source with an emission of 6.5×10^4 neutrons per second at a distance of 50 cm, centered, and for a total duration of 440 min (220 min in mask and 220 min in anti-mask positions). This image consists of around 7 000 events classified as neutrons, PSD value higher than 0.32 according to Fig. 16. We applied a threshold at zero to the density neutron image. The experiment confirmed the possibility of functional neutron imaging with a relatively short acquisition time. Any type of interference or misleading artifact remains well below half the maximum to the density neutron image.

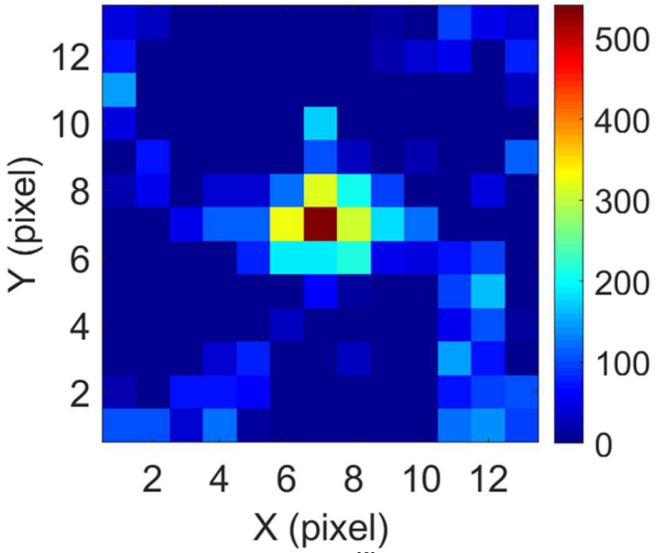

Fig. 21. Density neutron image of a ^{252}Cf source with an emission of 6.5×10^4 neutrons per second at a distance of 50 cm with 2×220 min acquisition times. Colorbars unit: reconstructed events.

C. Gamma source response

To our surprise, gamma imaging was also feasible. The coded mask was not designed to locate gamma sources, but it was still achievable. Fig. 22 shows the result obtained with the ^{133}Ba gamma source at a distance of 50 cm, centered, and for a total duration of 4 min (2 min in mask and 2 min in anti-mask positions). This image consists of around 20 000 events classified as photons, PSD value lower than 0.32 according to Fig. 16. We applied the same threshold at zero to the density neutron image. The image starts to be marked by reconstruction artifacts but the localization of the source remains possible.

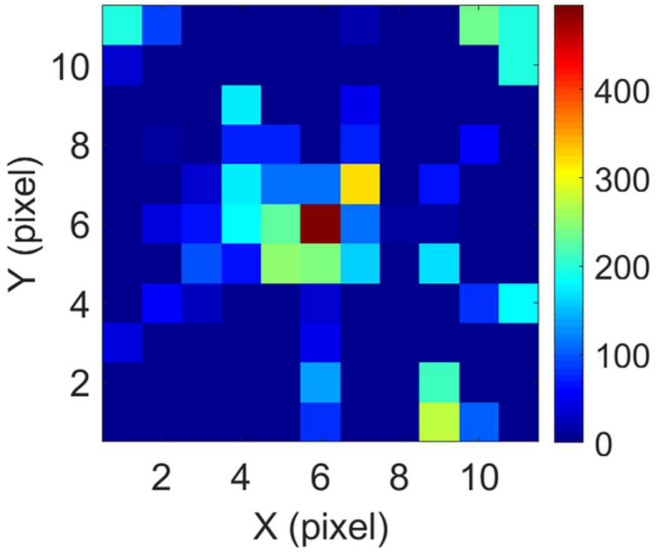

Fig. 22. Density gamma image of a ^{133}Ba source with an activity of 19.5 MBq at a distance of 50 cm with 2×2 min acquisition times. Colorbars unit: reconstructed events.

V. Conclusions

In this study, the use of pixelated plastic scintillators coupled with silicon photomultipliers applied to coded aperture gamma-

neutron imaging was investigated by Monte-Carlo simulation and experimental implementation.

In its prototype configuration, the gamma-neutron imager has a field of view of 68°, a spatial resolution of 7° and a gain in neutron detection efficiency of around 100 compared to the previous version [29]. Moreover, thanks to the multiplexing readout, the numbers of signals from the SiPM array to be digitized was reduced to five signals. This provides a major simplification of the back-end electronics required for the SiPM matrix reported in the literature [12]–[16]. It was experimentally verified that this multiplexing readout is able to discriminate and localize neutrons interaction within the PS. Finally, on the basis of the results obtained, it can be concluded that the acquisition chain studied in this work provides the possibility of locating and characterizing radioactive sources thanks to a pixelated plastic scintillators coupled with silicon photomultipliers and associated with a coded aperture.

Next experimental studies will include the measurement of the intrinsic gain of SiPMs and their temperature dependence in order to equalize the response within the array. Further characterizations should allow an optimization of the position-sensitive neutron detector. Homogenization of the gain with correcting factors should lead to a better energy calibration, spatial resolution and uniformity, gamma and neutron sensitivity and discrimination. Future work will focus on two main points: the pixelated PS scale up and the signals readout (hardware and software). We intend to increase the area and thickness of the detector as well as its number of pixels, and to develop a miniaturized electronic readout with embedded data processing.

REFERENCES

[1] C. Frangville, M. Hamel, G. H. V. Bertrand, E. Montbarbon, A. Grabowski, and C. Lynde, "Large solubility of lithium carboxylates reaching high rates of ^{6}Li incorporation in polystyrene-based plastic scintillators for fast/thermal neutron and gamma ray detection," *Mater. Chem. Front.*, vol. 3, no. 8, pp. 1626–1631, 2019.

[2] K. Amgarou *et al.*, "A comprehensive experimental characterization of the iPIX gamma imager," *J. Instrum.*, vol. 11, no. 8, pp. 377–381, 2016.

[3] C. G. Wahl *et al.*, "The Polaris-H imaging spectrometer," *Nucl. Instruments Methods Phys. Res. A*, vol. 784, pp. 377–381, 2015.

[4] S. Takeda *et al.*, "A portable Si / CdTe Compton camera and its applications to the visualization of radioactive substances," *Nucl. Instruments Methods Phys. Res. A*, vol. 787, pp. 207–211, 2015.

[5] M. Woodring *et al.*, "Advanced multi-dimensional imaging of gamma-ray radiation," *Nucl. Instruments Methods Phys. Res. Sect. A Accel. Spectrometers, Detect. Assoc. Equip.*, vol. 505, no. 1–2, pp. 415–419, 2003.

[6] G. Montemont *et al.*, "NuVISION: A Portable Multimode Gamma Camera based on HiSPECT Imaging Module," *2017 IEEE Nucl. Sci. Symp. Med. Imaging Conf. NSS/MIC 2017 - Conf. Proc.*, no. March, 2018.

[7] R. G. Johnson, J. W. Behrens, and C. D. Bowman, "Source Imaging Using Neutron Pinhole Cameras Based on Position Sensitive Proportional Counters," *Nucl. Technol.*, vol. 55, pp. 724–727, 1981.

[8] M. C. Hamel, J. K. Polack, A. Poitrasson-Rivière, S. D. Clarke, and S. A. Pozzi, "Localization and spectral isolation of special nuclear material using stochastic image reconstruction," *Nucl. Instruments Methods Phys. Res. A*, vol. 841, pp. 24–33, 2017.

[9] J. S. Beaumont, B. A. Shippen, M. P. Mellor, and M. J. Joyce, "Imaging of fast neutrons and gamma rays from 252Cf in a heavily shielded environment," *Nucl. Inst. Methods Phys. Res. A*, 2016.

[10] M. J. Cieślak, K. A. A. Gamage, R. Glover, and C. J. Taylor, "Gamma-ray modulation properties of tungsten coded apertures for a novel mixed-field imaging system," *J. Instrum.*, vol. 14, no. 2, 2019.

[11] X. Pang, Z. Zhang, J. Zhang, W. Zhou, Y. Zhang, and D. Cao, "A compact MPPC-based camera for omnidirectional (4pi) fast-neutron imaging based on double neutron – proton elastic scattering," *Nucl. Inst. Methods Phys. Res. A*, vol. 944, no. July, p. 162471, 2019.

[12] V. A. Li *et al.*, "A prototype for SANDD: A highly-segmented pulse-shape-sensitive plastic scintillator detector incorporating silicon photomultiplier arrays," *Nucl. Instruments Methods Phys. Res. Sect. A Accel. Spectrometers, Detect. Assoc. Equip.*, vol. 942, no. July, p. 162334, 2019.

[13] J. Boo, M. D. Hammig, and M. Jeong, "Hand-held dual-particle imager implemented with a multiplexed low sampling-rate readout of a SiPM-based pixelated stilbene array," *Res. Sq.*, 2020.

[14] W. M. Steinberger *et al.*, "Imaging Special Nuclear Material using a Handheld Dual Particle Imager," *Sci. Rep.*, pp. 1–11, 2020.

[15] H. Al Hamrashdi, D. Cheneler, and S. D. Monk, "A fast and portable imager for neutron and gamma emitting radionuclides," *Nucl. Instruments Methods Phys. Res. Sect. A Accel. Spectrometers, Detect. Assoc. Equip.*, vol. 953, no. September 2019, p. 163253, 2020.

[16] M. A. Wonders and M. Flaska, "Application of an added-sinusoid, signal-multiplexing scheme to a compact, multiplexed neutron scatter camera," *Nucl. Inst. Methods Phys. Res. A*, vol. 1002, no. June 2020, p. 165294, 2021.

[17] S. R. Gottesman and E. E. Fenimore, "New family of binary arrays for coded aperture imaging," *Appl. Opt.*, vol. 28, p. 4344, 1989.

[18] H. Lemaire *et al.*, "Implementation of an imaging spectrometer for localization and identification of radioactive sources," *Nucl. Inst. Methods Phys. Res. A*, vol. 763, pp. 97–103, 2014, doi: 10.1016/j.nima.2014.05.118.

[19] SensL, "C-series Low Noise, Blue-Sensitive Silicon Photomultipliers datasheet." pp. 1–17, 2016.

[20] F. H. Fröhner, "Evaluation of ^{252}Cf Prompt Fission Neutron Data from 0 to 20 MeV by Watt Spectrum Fit," *Nucl. Sci. Eng.*, vol. 106, no. 3, pp. 345–352, Nov. 1990.

[21] U. B. Jayanthi and J. Braga, "Physical implementation of an antimask in URA based coded mask systems," *Nucl. Instruments Methods Phys. Res. A*, vol. 310, pp. 685–689, 1991.

[22] G. H. V. Bertrand, M. Hamel, S. Normand, and F. Sguerra, "Pulse shape discrimination between (fast or thermal) neutrons and gamma rays with plastic scintillators: State of the art," *Nucl. Instruments Methods Phys. Res. Sect. A Accel. Spectrometers, Detect. Assoc. Equip.*, vol. 776, pp. 114–128, 2015.

[23] James Proffitt, "Diode enhanced amplifier circuits and methods thereof," 2013.

[24] S. Majewski, J. Proffitt, A. Stolin, and R. Raylman, "Development of a 'resistive' readout for SiPM arrays," *IEEE Nucl. Sci. Symp. Conf. Rec.*, vol. 9059, pp. 3939–3944, 2011.

[25] V. Popov, S. Majewski, and A. G. Weisenberger, "Readout electronics for multianode photomultiplier tubes with pad matrix anode layout," *IEEE Nucl. Sci. Symp. Conf. Rec.*, vol. 3, pp. 2156–2159, 2003.

[26] H. O. Anger, "Scintillation camera," *Rev. Sci. Instrum.*, vol. 29, pp. 27–33, 1958.

[27] D. Wolski, M. Moszyński, T. Ludziejewski, A. Johnson, W. Klamra, and Ö. Skeppstedt, "Comparison of n-γ discrimination by zero-crossing and digital charge comparison methods," *Nucl. Instruments Methods Phys. Res. Sect. A Accel. Spectrometers, Detect. Assoc. Equip.*, vol. 360, no. 3, pp. 584–592, 1995.

[28] C. Lynde *et al.*, "Optimization of the charge comparison method for multi-radiation field using various measurement systems," *IEEE Trans. Nucl. Sci.*, vol. 9499, no. c, pp. 1–9, 2020.

[29] C. Lynde *et al.*, "Demonstration of coded-aperture fast-neutron imaging based on Timepix detector," *Nucl. Instruments Methods Phys. Res. A*, no. July, 2018.